Scalar dispersion in a periodically reoriented potential flow: Acceleration via Lagrangian chaos

D. R. Lester* and M. Rudman
CSIRO Mathematical and Information Sciences, Locked Bag 33, Clayton South, Victoria 3169, Australia

G. Metcalfe
CSIRO Materials Science and Engineering, P.O. Box 56, Highett, Victoria 3190, Australia

M. G. Trefry†
CSIRO Land and Water, Underwood Avenue, Floreat, Western Australia 6014, Australia

A. Ord
School of Earth and Environment, University of Western Australia, 35 Stirling Highway Crawley, Western Australia 6009, Australia

B. Hobbs†
CSIRO Petroleum Resources, ARRC, 26 Dick Perry Avenue, Kensington, Western Australia 6151, Australia
(Received 12 November 2009; published 29 April 2010)

Although potential flows are irrotational, Lagrangian chaos can occur when these are unsteady, with rapid global mixing observed upon flow parameter optimization. What is unknown is whether Lagrangian chaos in potential flows results in accelerated scalar dispersion, to what magnitude, how robustly, and via what mechanisms. We consider scalar dispersion in a model unsteady potential flow, the Lagrangian topology of which is well understood. The asymptotic scalar dispersion rate q and corresponding scalar distribution (strange eigenmode) are calculated over the flow parameter space $\mathcal{Q}$ for Peclét numbers $\mathrm{Pe}=10^1-10^4$. The richness of solutions over $\mathcal{Q}$ increases with Pe, with pattern mode locking, symmetry breaking transitions to chaos and fractally distributed maxima observed. Such behavior suggests detailed global resolution of $\mathcal{Q}$ is necessary for robust optimization, however localization of local optima to bifurcations between periodic and subharmonic eigenmodes suggests novel efficient means of optimization. Acceleration rates of 150 fold at $\mathrm{Pe}=10^4$ are observed; significantly greater than corresponding values for chaotic Stokes flows, suggesting significant scope for dispersion acceleration in potential flows in general.

DOI: 10.1103/PhysRevE.81.046319 PACS number(s): 47.52.+j, 05.45.−a, 47.51.+a

I. INTRODUCTION

Over a quarter of a century ago, Aref [1] recognized that the kinematic advection equation

$$\dot{\mathbf{x}} = \mathbf{v}(\mathbf{x},t), \tag{1}$$

describing evolution of the position $\mathbf{x}$ of a passive tracer over time t in a fluid velocity field $\mathbf{v}$ represents a dynamical system rich enough to exhibit chaotic dynamics, even in the limit of vanishing Reynolds number. This phenomena, termed *chaotic advection* [2] or *Lagrangian chaos* has important implications for fluidic mixing and scalar transport, and has been exploited in a wide range of applications. It has been demonstrated [3] that chaotic dynamics can significantly increase the rate of dispersion of diffusive scalars in Stokes flows, facilitating accelerated heat transfer [4], diffusive mixing [5], chemical reaction [6], and low Reynolds number scalar transport in general [7].

Despite the irrotational nature of potential flows, it has more recently been demonstrated computationally [8,9] and experimentally [10–12] that Lagrangian chaos can also occur in unsteady potential flows via the transient crossing of streamlines. To our knowledge there exist only a handful of papers [8–14] dealing with Lagrangian chaos in potential flows, and an outstanding question is whether scalar dispersion acceleration via Lagrangian chaos also extends to such flows. Furthermore, what magnitude accelerations are possible, how robust are the phenomena, and what are the governing mechanisms of dispersion acceleration in potential flows?

For a given flow geometry, an open question is what forcings and/or perturbations generate global Lagrangian chaos and optimal scalar transport. To date, no investigation of dispersion optimization via simultaneous diffusion and Lagrangian chaos has been performed for potential flows.

These questions are also of direct relevance to transport in porous media, the *macroscopic* fluid mechanics of which are described by the Darcy equation as a potential flow. Applications in porous media include geothermal energy, *in situ* mining, contaminated site remediation, and shale oil recovery, and Lagrangian chaos is also relevant to understanding geophysical transport phenomena in processes such as ore body formation and mineral deposition. Although this study makes no claim as to direct modeling of porous media applications, coupled potential flow advection and Brownian diffusion represents a scalar transport mechanism qualitatively similar to that of porous media at the macroscale. In particular, transport in porous media differs in that heterogeneities

*daniel.lester@csiro.au
†University of Western Australia, School of Earth and Environment, 35 Stirling Highway Crawley, WA 6009

 ©2010 The American Physical Society

in porosity and permeability alter the transport and Darcy equations, respectively, and furthermore scalar diffusion manifests as a hydrodynamic dispersion which is often anisotropic and several orders of magnitude larger than the underlying molecular diffusion. As is argued in Sec. IV, such differences do not change the qualitative fundamentals of scalar dispersion acceleration in potential flows.

Hydrodynamic dispersion in porous media at the *macroscale* arises from the coupling of molecular diffusion with Lagrangian chaos (via Stokesian microflows) generated by the tortuosity of porous media at the *microscale*. The primary difference between Lagrangian chaos in porous media at the microscale and macroscale is that the former case arises naturally from Stokes flow within the geometrically complex pore space and so cannot be controlled, whereas the latter may be invoked and controlled by judicious "programming" of macroscopic flows as approximated by the Darcy equation. In general, scalar dissipation (whether driven by hydrodynamic dispersion or Brownian diffusion) of any magnitude dramatically alters the dynamics of chaotic advection [3], and so hydrodynamic dispersion can rarely be ignored in chaotic porous media flows.

In this paper we consider scalar transport resulting from combined diffusion (as modeled by the Laplacian operator) and advection in potential flows. Specifically we consider scalar transport in a two-dimensional (2D) unsteady model potential flow to examine the nature of scalar dispersion acceleration via Lagrangian chaos. This model flow contains several flow control parameters, which form a multidimensional parameter space $\mathcal{Q}$ over which the Lagrangian dynamics can vary significantly [8]. Dispersion problems also involve the Peclét number, $\mathrm{Pe}=LV/D$, where L, V respectively are the characteristic length and velocity scales of the system and D is diffusivity, with Pe quantifying the relative time scales of advection to diffusion. We wish to resolve scalar transport over the parameter space $\mathcal{Q}\times\mathrm{Pe}$ to elucidate the global structure of transport in this model system.

Evidence [15] from chaotic Stokes flows suggests that the rate of scalar dispersion may exhibit rich fractal-like behavior over $\mathcal{Q}\times\mathrm{Pe}$, hence it is anticipated that such behavior extends to chaotic potential flows. In this work we globally resolve this space to high precision to determine the optimum level of scalar dispersion enhancement in the model potential flow and identify relevant governing mechanisms. By establishing the applicability of these results to potential flows in general as well as more complex porous media, we can determine the scope for dispersion enhancement for a wide range of porous media applications.

II. PROBLEM DEFINITION

A. Scalar dispersion in potential flows

To study scalar dispersion in potential flows, we consider the evolution of a diffusive scalar ϕ in an arbitrary flow domain $\mathcal{D}$, governed by the advection-diffusion equation (ADE)

$$\frac{\partial\phi}{\partial t}+\mathbf{v}\cdot\boldsymbol{\nabla}\phi=\frac{1}{\mathrm{Pe}}\boldsymbol{\nabla}^2\phi, \tag{2}$$

subject to the initial conditions $\phi(\mathbf{x},0)=\phi_0(\mathbf{x})$ (where $\int_{\mathcal{D}}\phi_0 d^2\mathbf{x}=0$ without loss of generality) and homogeneous Neumann boundary conditions $\mathbf{n}\cdot\boldsymbol{\nabla}\phi|_{\partial\mathcal{D}}=0$, where $\mathbf{n}$ is the unit normal outward vector on $\partial\mathcal{D}$. To resolve the global parametric structure of scalar transport, we need to resolve the dispersion rate generated by the ADE over the flow parameter space $\mathcal{Q}$ for various values of the Peclét number Pe. Previous studies [7,8,15] have shown complex fractal-like distributions of solutions to Eq. (2) over the parameter space $\mathcal{Q}$ for reoriented Stokes flows, and so it is anticipated that similar behavior may occur in potential flows. As such, efficient methods are required to resolve $\mathcal{Q}$ to high resolution, and so we employ the composite spectral method [15]. This method does not seek to directly solve (2), but rather determines the dominant "strange eigenmodes" [16–18] φ_k of the advection-diffusion operator $\mathcal{L}[\varphi]=-\mathbf{v}\cdot\boldsymbol{\nabla}\varphi+1/\mathrm{Pe}\boldsymbol{\nabla}^2\varphi$, over $\mathcal{Q}$ such that

$$\phi(\mathbf{x},t)=\sum_{k=0}^{K}\alpha_k(t)\varphi_k(\mathbf{x},t)e^{\lambda_k t}, \tag{3}$$

where $\alpha_k(t)$ are the eigenmode weights (which may be unsteady due to the non-self adjoint nature of $\mathcal{L}$ [19]) arising from the initial condition ϕ_0, λ_k are the eigenvalues of $\mathcal{L}$, and k is ordered such that $\mathrm{Re}(\lambda_k)\leq\mathrm{Re}(\lambda_{k+1})$, with all $\mathrm{Re}(\lambda_k)$ negative. For velocity fields $\mathbf{v}$ which are T periodic in time, the strange eigenmodes are also T periodic, and so in this case are in essence the Floquet modes of the $\mathcal{L}$ operator. For sufficiently long times, the most slowly decaying mode persists:

$$\phi(\mathbf{x},t)\rightarrow\phi_\infty(\mathbf{x},t)=\alpha_0(t)\varphi_0(\mathbf{x},t)e^{\lambda_0 t}, \tag{4}$$

hence the asymptotic decay rate of the scalar field ϕ is quantified by $|\lambda_0|$. Note that generally as more of the initial signal ϕ_0 is projected onto the most regular (i.e., lowest variance) eigenmode, there is a tendency for $|\alpha_0(0)|>|\alpha_k(0)|$, and furthermore scalar variance is preferentially transferred from $\alpha_k\rightarrow\alpha_0$ with time [19] due to $\mathcal{L}$ being nonself-adjoint. As such, λ_0 not only represents an exact measure of scalar dispersion in the asymptotic limit $t\rightarrow\infty$, but in general is also a useful approximation of dispersion for all but short times $t\lesssim 1/(|\lambda_1|-|\lambda_0|)$.

The nonself-adjoint nature of $\mathcal{L}$ also admits complex eigenmodes, realized as conjugate pairs $\varphi_k=\varphi_k^r\pm i\varphi_k^i$ and $\lambda_k=\lambda_k^r\pm i\lambda_k^i$. Hence the conjugate eigenmode pair manifests in real space as

$$\varphi_k^*(\mathbf{x},t)e^{\lambda_k^r t}=\alpha_k(t)\{\varphi_k^r(\mathbf{x},t)\cos[\lambda_k^i(t-t_k)]+\varphi_k^i(\mathbf{x},t)\sin[\lambda_k^i(t-t_k)]\}e^{\lambda_k^r t}, \tag{5}$$

where both $\alpha_k(t)$ and t_k are dictated by the initial conditions. As φ_k^r and φ_k^i may only be T periodic in time, complex pairs give rise to two superposed eigenmodes $(\varphi_k^r,\varphi_k^i)$ separated in time by phase angle $\pi/2$, which are either subharmonic or quasiperiodic depending upon whether λ_k^i is commensurate with π/T. From Eq. (5), the asymptotic scalar dispersion rate for complex eigenmodes is $\lambda_0^r=\mathrm{Re}[\lambda_0]$.

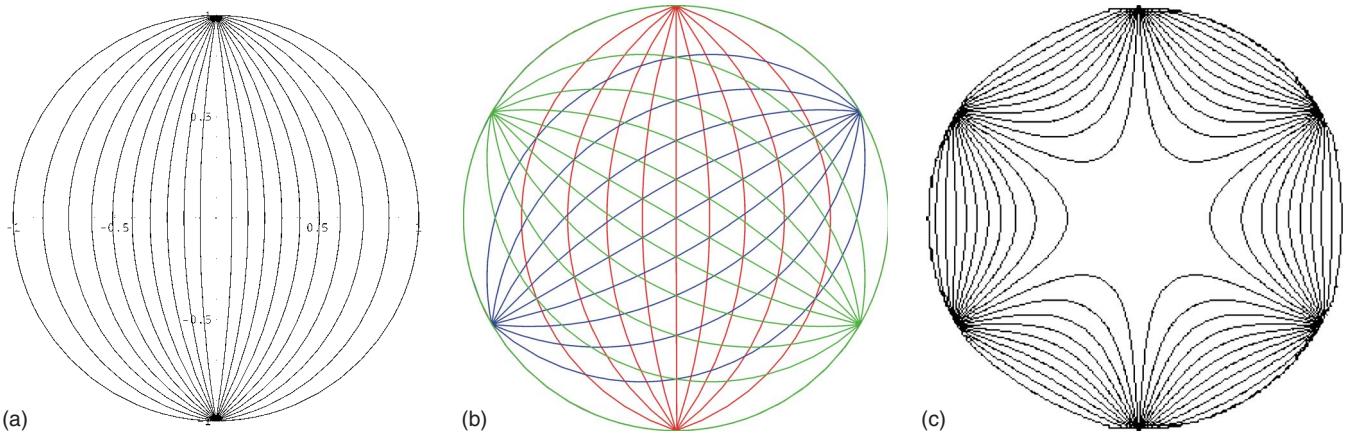

FIG. 1. (Color online) (a) Contours of dipole flow stream function with inlet (outlet) $\mathbf{x}^+$ ($\mathbf{x}^-$) at $r=1$, $\theta=\pi/2$ ($\theta=-\pi/2$). (b) Superposed streamlines of the RPM flow for $\Theta=2\pi/3$ and (c) corresponding Hamiltonian H in the singular limit $\tau\to 0$.

Calculation of the dominant eigenmode φ_0 and associated eigenvalue λ_0 using the composite spectral method [15] for the ADE resolves the asymptotic rate of scalar dispersion and the associated dominant decaying pattern over the parameter space $\mathcal{Q}\times \mathrm{Pe}$.

B. Rotated potential mixing flow

As the mixing properties and Lagrangian topology of the so-called rotated potential mixing (RPM) flow are well understood [8], this flow serves as a convenient model for the study of scalar dispersion in potential flows. The RPM flow is based upon a simple dipole flow arising from a source (+) and sink (−) located at $\mathbf{x}^+:\{r,\theta\}=(1,\pi/2)$ and $\mathbf{x}^-:\{r,\theta\}=(1,-\pi/2)$, respectively, as depicted in Fig. 1(a). The flow domain $\mathcal{D}:\{r,\theta\}=[0,1]\times[-\pi,\pi]$ under consideration is bounded on $\partial\mathcal{D}$ by the separating streamlines at $r=1$, and we consider the RPM flow in *closed* mode, such that a particle which exits the sink $\mathbf{x}^-$ is instantaneously re-injected at the source $\mathbf{x}^+$ with the corresponding streamnumber preserved. Although instantaneous reinjection is nonphysical, the addition of a time delay to the reinjection protocol does not alter the Lagrangian topology of the system [8]. The source-sink pair sets up a dipole flow with stream function ψ

$$\psi(r,\theta)=\arctan\left(\frac{2r\cos\theta}{1-r^2}\right), \tag{6}$$

generating the flow velocity $\hat{\mathbf{v}}=\boldsymbol{\nabla}\times\psi\hat{\mathbf{e}}_z$, where $\hat{\mathbf{e}}_z$ is the unit vector normal to $\mathcal{D}$. The simplest stirring protocol to introduce transient crossings of streamlines is to let $\hat{\mathbf{v}}$ operate for some time τ, after which the dipole positions are instantaneously reoriented about the origin through angle Θ. This reoriented flow operates for time τ, then is further reoriented by Θ, and so on. This unsteady flow is the RPM flow, the streamlines of which are depicted in Fig. 1(b), and the RPM velocity field is approximately

$$\mathbf{v}(\mathbf{x},t;\tau,\Theta)\approx\hat{\mathbf{v}}\left(r,\theta+\left\lfloor\frac{t}{\tau}\right\rfloor\Theta\right), \tag{7}$$

where $\lfloor x\rfloor$ denotes the integer part of x. The approximation (7) is exact for finite τ in the limit of vanishing Reynolds number Re. Note that the RPM flow is temporally periodic with period $T=j\tau$ for rational $\Theta/2\pi=k/j$, with integers k, j. The adjustable flow parameters τ, Θ for the RPM flow form the flow parameter space $\mathcal{Q}:\{\tau,\Theta\}=[0,\infty)\times[\pi,\pi]$ over which the Lagrangian dynamics vary significantly [8]. The RPM flow has been experimentally realized [10,11] and dye advection experiments were found to agree very well with theory.

As the flow field is divergence-free ($\boldsymbol{\nabla}\cdot\mathbf{v}=0$), the system (1) is conservative (Hamiltonian), such that the unsteady Hamiltonian H corresponds to the reoriented stream function

$$H=\psi\left(r,\theta+\left\lfloor\frac{t}{\tau}\right\rfloor\Theta\right). \tag{8}$$

In the limit $\tau\to 0$, the Hamiltonian is steady and equivalent to the time-averaged reoriented stream function:

$$H=\begin{cases}\dfrac{1}{j}\displaystyle\sum_{n=0}^{j-1}\psi(r,\theta-n\Theta) & \text{for}\quad \Theta=2\pi\dfrac{k}{j},\\[2ex] \displaystyle\int_{-\pi}^{\pi}\psi(r,\theta)d\theta & \text{for}\quad \text{irrational}\dfrac{\Theta}{\pi},\end{cases} \tag{9}$$

as is depicted in Fig. 1(c) for $\Theta=2\pi/3$. Note that due to the reflection-reversal symmetry $\hat{\mathbf{v}}(r,\theta)=-\hat{\mathbf{v}}(r,\theta+\pi)$, H in this limit is identically zero for all cases in (9) except for rational Θ where the denominator j is odd.

Following the previous subsection, we define the rate of scalar transport *enhancement* q in the RPM flow as the ratio of λ_0 between the unrotated case ($\Theta=0$) and that for a particular stirring protocol Θ, τ

$$q\equiv\frac{\mathrm{Re}[\lambda_0]}{\mathrm{Re}[\lambda_0|_{\Theta=0}]}, \tag{10}$$

where the reference case $\lambda_0|_{\Theta=0}$ only changes with Pe. A lower bound for q is given by the slowest decaying Laplacian eigenmode over $\mathcal{D}$ (with $\beta_{1,1}$ is the first zero of $J_1'(r)$, the first order Bessel function of the first kind)

$$q_{\min}=-\frac{1}{\mathrm{Pe}}\frac{\beta_{1,1}^2}{\mathrm{Re}[\lambda_0|_{\Theta=0}]}<1, \tag{11}$$

and so it is potentially possible to *retard* transport in the RPM flow with respect to the base dipole flow ($\Theta=0$).

III. NUMERICAL METHOD

We require a method to calculate $\varphi_0(\mathbf{x})$ and λ_0 efficiently over the parametric space $\mathcal{Q}\times\mathrm{Pe}$. The composite spectral method [15] achieves this by exploiting the symmetries inherent to the RPM flow (7) to rapidly construct a spectral representation of the AD operator $\mathcal{L}$ projected over one period τ in the form of the matrix operator $\mathbf{S}^\star$. Solution of the dominant eigenvector and eigenvalue of $\mathbf{S}^\star$ corresponds to spectral approximations of the dominant eigenmode φ_0 and eigenvalue λ_0. Implementation of this method for the RPM flow is briefly outlined as follows.

The Laplacian eigenfunctions $\omega_n(\mathbf{x})$ over $\mathcal{D}$ with homogeneous Neumann boundary conditions serve as basis functions for spectral expansion of the scalar field ϕ. These functions are ordered in terms of increasing Laplacian eigenvalue μ_n^2, and the expansion is truncated at N terms $\phi(\mathbf{x},t)=\sum_{n=0}^{N-1}\Phi_n(t)\omega_n(\mathbf{x})$, with the length N vector of expansion coefficients $\Phi_n(t)$ denoted $\mathbf{\Phi}$. The minimum size N of the spectral basis is ultimately dictated by the variance of the dominant eigenmode φ_0, and so is expected to increase with Pe. The ADE (2) may be represented spectrally as

$$\frac{d\mathbf{\Phi}}{dt}=\left(\mathbf{H}_{\Theta,\tau}(t)-\frac{1}{\mathrm{Pe}}\mathbf{D}\right)\cdot\mathbf{\Phi}=\mathbf{A}(t)\cdot\mathbf{\Phi}, \tag{12}$$

where $\mathbf{H}_{\Theta,\tau}(t)$ is an $N\times N$ matrix representing the advection operator $-\mathbf{v}\cdot\boldsymbol{\nabla}$, and $\mathbf{D}$ is the spectral diffusion operator comprising of a constant diagonal $N\times N$ matrix of eigenvalues μ_n^2. As the RPM velocity $\mathbf{v}$ is piecewise constant in time, $\mathbf{H}$ is likewise, such that

$$\mathbf{H}_{\Theta,\tau}(t)=\mathbf{R}_\Theta^{\lfloor t/\tau\rfloor-1}\cdot\hat{\mathbf{H}}\cdot\mathbf{R}_\Theta^{1-\lfloor t/\tau\rfloor}, \tag{13}$$

where $\mathbf{R}_\Theta$ is the operator associated with a rotation of the solution through angle Θ, and $\hat{\mathbf{H}}$ is the spectral representation of the operator $-\hat{\mathbf{v}}\cdot\boldsymbol{\nabla}$.

The fundamental matrix solution $\mathbf{S}(t)$ to Eq. (12) is

$$\mathbf{S}(t)=\exp\left\{\int_0^t\mathbf{A}(\zeta)d\zeta\right\}, \tag{14}$$

where

$$\mathbf{\Phi}(t)=\mathbf{S}(t)\cdot\mathbf{\Phi}(0), \tag{15}$$

$$\frac{d\mathbf{S}}{dt}=\mathbf{A}(t)\cdot\mathbf{S}(t). \tag{16}$$

From Eq. (12), $\mathbf{A}(t)$ is piecewise steady and so Eq. (14) may be decomposed as

$$\mathbf{S}(n\tau)=\exp\{(\mathbf{R}_\Theta^{n-1}\cdot\mathbf{A}_0\cdot\mathbf{R}_\Theta^{1-n})\tau\}\cdot\ \ldots\ \cdot\exp\{(\mathbf{R}_\Theta\cdot\mathbf{A}_0\cdot\mathbf{R}_\Theta^{-1})\tau\}\cdot\exp\{\mathbf{A}_0\tau\}, \tag{17}$$

for any integer n, where $\mathbf{A}_0=\mathbf{A}(0)$. The rotation operations $\mathbf{R}_\Theta^j\cdot\mathbf{A}_0\cdot\mathbf{R}_\Theta^{-j}$ in Eq. (17) represent a similarity transform, and thus commute with the exponential operator, resulting in the simplified expression

$$\mathbf{S}(n\tau)=\mathbf{R}_\Theta^n\cdot(\mathbf{R}_\Theta^{-1}\cdot\exp\{\mathbf{A}_0\tau\})^n. \tag{18}$$

As such, eigenanalysis of the advection-diffusion operator can be performed over a single offset period τ, where $\mathbf{S}^\star$ is the matrix solution operator over time τ in a frame moving with the dipole

$$\mathbf{S}^\star=\mathbf{R}_\Theta^{-1}\cdot\exp\left\{\left(\hat{\mathbf{H}}-\frac{1}{\mathrm{Pe}}\mathbf{D}\right)\tau\right\}. \tag{19}$$

Using this expression, the spectral coefficients of the dominant eigenmode at $\tau=0$ $\varphi_0^\star(\mathbf{x},0)$ (in the dipole frame) and associated decay rate $\exp\{-\lambda_0\tau\}$ are, respectively, given by the dominant eigenvector and eigenvalue of $\mathbf{S}^\star$. Simplification to Eq. (19) obviates the need to calculate the full fundamental solution $\mathbf{S}(T)$, which is expensive for large j and impossible for irrational values of Θ/π. Spectral representation of the advection operator $\hat{\mathbf{H}}$ can involve a significant computational effort, however $\hat{\mathbf{H}}$ needs only to be calculated once, with the parameters τ, Θ, and Pe varied independently as per Eq. (19).

The coefficients of $\hat{\mathbf{H}}$ are calculated as

$$\hat{\mathbf{H}}_{j,k}=\int_{\mathcal{D}}\omega_k(\mathbf{x})\hat{\mathbf{v}}(\mathbf{x})\cdot\boldsymbol{\nabla}\omega_j(\mathbf{x})d^n\mathbf{x}, \tag{20}$$

which may be simplified by using $\hat{\mathbf{v}}=\boldsymbol{\nabla}\times\boldsymbol{\psi}$, $\boldsymbol{\psi}=\psi\hat{\mathbf{e}}_z$ with the identity

$$\omega_j(\boldsymbol{\nabla}\times\boldsymbol{\psi})\cdot\boldsymbol{\nabla}\omega_k=\boldsymbol{\psi}\cdot(\boldsymbol{\nabla}\omega_j\times\boldsymbol{\nabla}\omega_k)-\boldsymbol{\nabla}\cdot(\boldsymbol{\nabla}\omega_k\times\boldsymbol{\psi}\omega_j), \tag{21}$$

to give

$$\hat{\mathbf{H}}_{j,k}=\int_{\mathcal{D}}\boldsymbol{\psi}\cdot(\boldsymbol{\nabla}\omega_j\times\boldsymbol{\nabla}\omega_k)d^n\mathbf{x}-\oint_{\partial\mathcal{D}}\mathbf{n}\cdot(\boldsymbol{\nabla}\omega_k\times\boldsymbol{\psi}\omega_j). \tag{22}$$

The first term on the right-hand side of Eq. (22) represents transfer between spectra within $\mathcal{D}$ and the second represents flux across the boundary $\partial\mathcal{D}$ which simplifies to

$$\int_{-\pi}^{\pi}\left(\omega_j\frac{\partial\omega_k}{\partial\theta}\psi\right)\ |_{r=1}d\theta \tag{23}$$

and is nonzero only for (ω_j,ω_k) either (odd, even) or (even, odd) with respect to θ. As this term represents the total scalar flux leaving domain $\mathcal{D}$, it is set to zero to emulate the RPM operating in *closed* mode, effectively forcing all scalar

exiting at $\mathbf{x}^-$ to be reinjected at $\mathbf{x}^+$.

The singular nature of these points poses a computational problem, and so they are excluded by reducing the computational domain to $\mathcal{D}_c:\{r,\theta\}=[0,1-10^{-3}]\times[-\pi,\pi]$. In essence, this operation changes the source/sink nature of $\mathbf{x}^+$, $\mathbf{x}^-$ to inflow/outflow boundaries in the neighborhood of $\mathbf{x}^+$, $\mathbf{x}^-$ on $\partial\mathcal{D}_c$, and the closure operation above [forcing Eq. (23) equal to zero] enforces periodic conditions (namely, reflection across $y=0$) upon these boundaries.

This symmetry of the dipole stream function (see Fig. 1) simplifies calculation of $\hat{H}_{j,k}$ as only combinations of ω_j, ω_k which are respectively even and odd in θ are nonzero. The θ component of the domain integral in Eq. (22) has analytic solutions for these combinations

$$\int_{-\pi}^{\pi}\psi(r,\theta)\cos(n\theta)\cos(p\theta)d\theta=\pi\begin{cases}n+p\ \text{ even} & 0,\\ n+p\ \text{ odd} & (-1)^{(|n-p|-1)/2}\dfrac{r^{|n-p|}}{|n-p|}+(-1)^{(|n+p|-1)/2}\dfrac{r^{|n+p|}}{|n+p|},\end{cases}\tag{24}$$

$$\int_{-\pi}^{\pi}\psi(r,\theta)\sin(n\theta)\sin(p\theta)d\theta=\pi\begin{cases}n+p\ \text{ even} & 0,\\ n+p\ \text{ odd} & (-1)^{(|n-p|-1)/2}\dfrac{r^{|n-p|}}{|n-p|}-(-1)^{(|n+p|-1)/2}\dfrac{r^{|n+p|}}{|n+p|},\end{cases}\tag{25}$$

and so only the r components of these integrals require numeric calculation. We exploit the recurrent nature of the orthogonal basis functions $\omega_n(\mathbf{x})$ by using the fast collocation method of Levin [20] to compute these integrals, using Chebyshev polynomials as a collocation basis.

Given calculation of $\hat{\mathbf{H}}$ for given N (dictated by Pe), the task remains to determine $\mathbf{S}^\star$ discretely over $\tau\in[\tau_{\min},\tau_{\max}]$ and $\Theta\in[-\pi,\pi]$ to resolution $M_\tau\times M_\Theta$, such that $\delta\tau=(\tau_{\min}-\tau_{\max})/M_\tau$ and $\delta\Theta=2\pi/M_\theta$. Construction of $\mathbf{A}_0$ is straightforward as $\mathbf{D}$ is sparse and analytic, and calculation of the matrix exponentials $\exp\{\delta\tau\mathbf{A}_0\}$, $\exp\{\tau_{\min}\mathbf{A}_0\}$ is performed efficiently via the fast integration method [21]. Subsequent time-stepping forward by $\delta\tau$ of the operator $\exp\{(\tau+\delta\tau)\mathbf{A}_0\}$ is achieved by matrix multiplication by $\exp\{\delta\tau\mathbf{A}_0\}$.

For each value of τ, Θ is varied from $-\pi$ to π in increments of $\delta\Theta$ such that $\mathbf{S}^\star=\mathbf{R}_{\delta\Theta}^{-1}\cdot\mathbf{S}^\star$, where the rotation operator $\mathbf{R}_{\delta\Theta}^{-1}$ is sparse and analytic. For each value of Θ, the dominant eigenvectors and eigenvalues of $\mathbf{S}^\star$ are then calculated via the Arnoldi method implemented in the AARPACK distribution, with the previously calculated eigenvector used as an initial guess to aid convergence. A target tolerance of 10^{-16} is generally achieved within 100 iterations when a Krylov subspace dimension of order 200 is used. As the operator $\mathcal{L}$ is nonself-adjoint, $\mathbf{S}^\star$ is real and asymmetric (with $\hat{\mathbf{H}}$ skew-symmetric and $\mathbf{D}$ diagonal) and so convergence of the Arnoldi method can be slow for large N, imposing a limit of application of the method for very large Pe, i.e., $\mathrm{Pe}\gtrsim 10^7$.

For $\mathrm{Pe}=10^1-10^4$, the computational space of interest $\mathcal{Q}_c:\{\tau,\Theta\}=[10^{-2},10^3]\times[-\pi,\pi]$ is broken down into subregions of $[\tau_{\min},\tau_{\max}]$ with different $\delta\tau$, $\delta\Theta$, depending on the level of resolution required, see Fig. 2. The calculated eigenvectors and eigenvalues represent spectral approximations of the dominant eigenmode $\varphi_0(\mathbf{x},t)$ and associated decay rate λ_0 of the $\mathcal{L}$ operator over the control parameter space $\mathcal{Q}\times\mathrm{Pe}$.

IV. RESULTS AND DISCUSSION

A. Scalar dispersion acceleration in the RPM flow

Distributions of the enhancement factor q over $\mathcal{Q}$ for $\mathrm{Pe}=10^1-10^4$ are illustrated in Fig. 2. The distribution of q is rich, with increasingly fine scale structure with Pe, and multiple local optima (maxima) across $\mathcal{Q}$. For all Pe, both the enhancement factor q and the underlying eigenmodes are symmetric in $\mathcal{Q}$ across $\Theta=0$ due to the double symmetry of the RPM flow [8], which is also reflected in symmetry of the Poincaré sections across $\Theta=0$. Note that due to this symmetry, only $\Theta\in[0,\pi]$ is shown in Fig. 2. However, the reflection-reversal symmetry [along the x axis in Fig. 1(a)] which manifests as a reflection symmetry along $\theta=-\Theta/2$ in Poincaré sections [8] does not persist for the strange eigenmodes due to the diffusion operator altering the orbits of scalar parcels. Aside from this symmetry, the distribution of q over $\mathcal{Q}$ shares many features with that of the chaotic Stokes flow of the rotated arc mixer [7,15].

For low values of τ, expansive ridges (and valleys) of increased (and decreased) q emanate from rational values of Θ/π along the $\tau=0$ axis. The distribution of these expansive tonguelike structures is similar [22] to that of Arnol'd tongues for frequency locking [23], which also emanate from rational values of the offset parameter for the standard circle map. Along the tonguelike structures in $\mathcal{Q}$ the corresponding eigenmodes are rotationally symmetric, with j-fold symmetric eigenmodes occurring at $\Theta=2\pi k/j$ for integers k, j as depicted in Fig. 3, and so tongues exhibit *mode locking* with respect to the offset angle Θ.

Mode locking is a direct consequence of the existence of a steady rotationally symmetric Hamiltonian H for rational Θ/π in the limit $\tau\to 0$, as given by Eq. (9) and illustrated in Fig. 1(c). The corresponding Poincaré sections for the kinematic problem (1) are also rotationally symmetric in $\tau\to 0$ [8]. As the Hamiltonian and velocity field $\mathbf{v}$ are steady in this

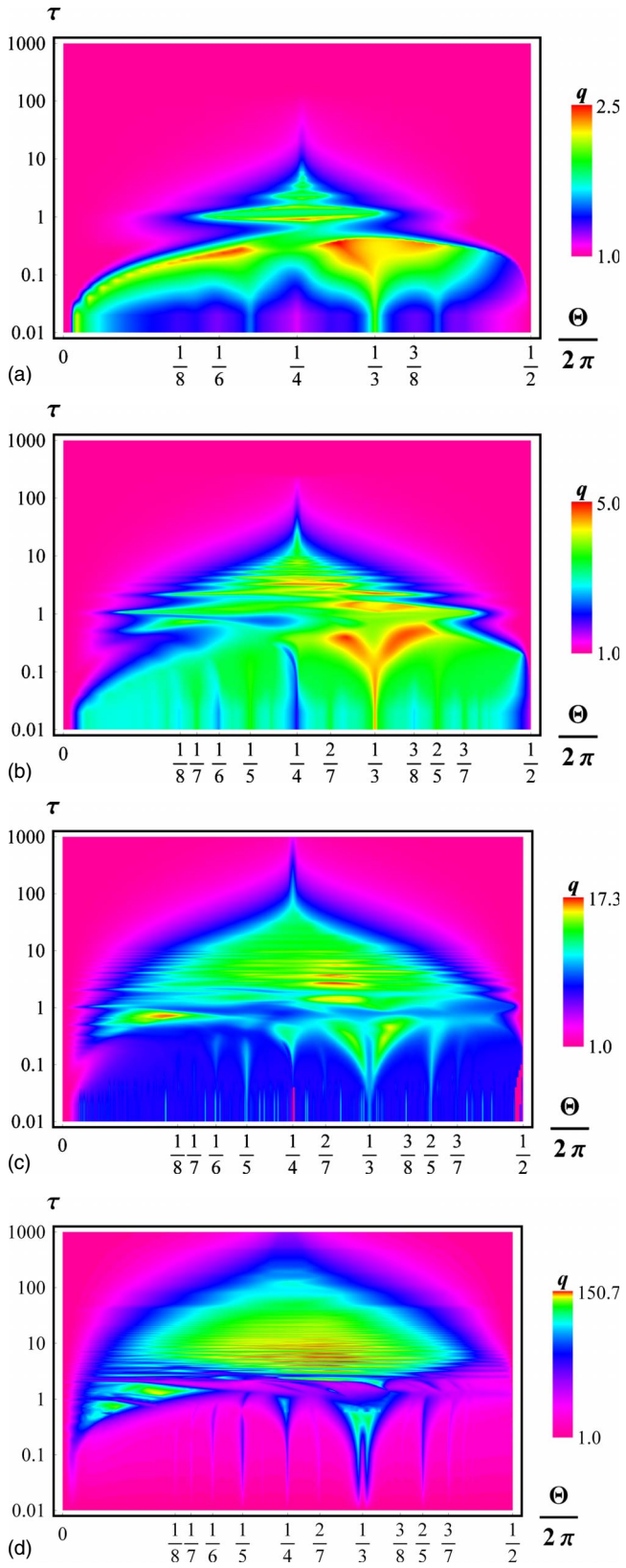

FIG. 2. (Color online) Distribution of the dispersion acceleration factor q over flow parameter space $\mathcal{Q}$ for (a) $\mathrm{Pe}=10^1$, (b) $\mathrm{Pe}=10^2$, (c) $\mathrm{Pe}=10^3$, and (d) $\mathrm{Pe}=10^4$. Note logarithmic scaling of contours in q in (c) and (d).

limit, the corresponding eigenmodes are likewise [albeit exponentially decaying as per (3)]. The form of these eigenmodes is "programmed" by the steady Hamiltonian, albeit smeared by diffusion, and toward the limit $\mathrm{Pe}\to\infty$, the eigenmode approaches the Hamiltonian itself. At low τ for either even j or irrational Θ/π, the time-averaged flow is zero, and so the ADE (2) is well-approximated by a diffusion equation, hence the dominant eigenmode is similar to the slowest decaying Laplacian eigenfunction and $\lambda_0 \sim \beta_{1,1}^2/\mathrm{Pe}$ or $q\sim 1$, as is most clearly reflected in Figs. 2(a) and 2(b). In this case, scalar transport is actually *retarded* with respect to the no-reorientation ($\Theta=0$) case as the unreoriented dipole flow generates some enhanced transport due to the velocity difference across neighboring streamlines. Such phenomena is evident in Fig. 4, which illustrates q along Θ for $\tau=0.01$ at $\mathrm{Pe}=10^1$. Local maxima occur around odd values of j, and minima around even values (with retardation ($q<1$ occurring at $j=2$), with the strength of these extrema decreasing with increasing j.

With increasing τ, the mode-locked tongues collide at some critical value τ_{crit}. Competing resonances between tongues lead to period-doubling bifurcations in the kinematic problem for $\tau>\tau_{\mathrm{crit}}$, and fully chaotic dynamics ensue at the accumulation point of the cascade [8], as is the case for the standard circle map. This route to chaos is reflected in the q distributions in Fig. 2, where an accumulation point around $\tau\sim 2$ is observed, at which point the mixing template generates space-filling Lagrangian chaos. For moderate values ($\mathrm{Pe}\lesssim 10^2$) of Pe, global (with respect to $\mathcal{Q}$) optima lie on the Arnol'd tongues for $\tau\lesssim 2$, but as Pe increases to the convection-dominated regime ($\mathrm{Pe}\gtrsim 10^3$), the optima move up above the accumulation point $\tau\sim 2$ as per Fig. 2.

This transition is associated with an evolution in the Lagrangian topology from globally regular (and rotationally symmetric in the Arnol'd tongues) to globally chaotic with increasing τ (as evidenced in the Poincaré sections [8]).

Why do the chaotic stirring protocols achieve less scalar dispersion acceleration than regular protocols for moderate or low Pe? Consider the eigenmode decay rate λ_0 in terms of the eigenmode variance $\|\bar{\varphi}_0\|^2$ and gradient variance $\|\nabla\bar{\varphi}_0\|^2$

$$\mathrm{Re}[\lambda_0] = \frac{1}{\mathrm{Pe}}\frac{\|\nabla\bar{\varphi}_0\|^2}{\|\bar{\varphi}_0\|^2}, \tag{26}$$

where $\|\cdot\|, \bar{\cdot}$ denote the L_2 norm over $\mathcal{D}$ and temporal average over τ, respectively [17]. As such, the rate of scalar dispersion is given by the average scalar gradient $\|\nabla\bar{\varphi}_0\|^2/\|\bar{\varphi}_0\|^2$, and as eigenmodes are *persistent*, the dispersion rate is dictated by the gradient which can be maintained. If the dominant eigenmode is represented spectrally as

$$\varphi_0(\mathbf{x},t)e^{\lambda_0 t} = \sum_n^\infty \alpha_n(t)\omega_n(\mathbf{x}), \tag{27}$$

then the coefficients $\alpha_1^2, \alpha_2^2, \ldots, \alpha_n^2$ represent a "scalar energy" spectrum of increasing wave number n, subject to the normalization $\Sigma_n^\infty \alpha_n(t)^2=1$. The decay rate λ_0 is directly governed by this spectrum, such that energy spectra weighted at high wave numbers decays faster than low wave number

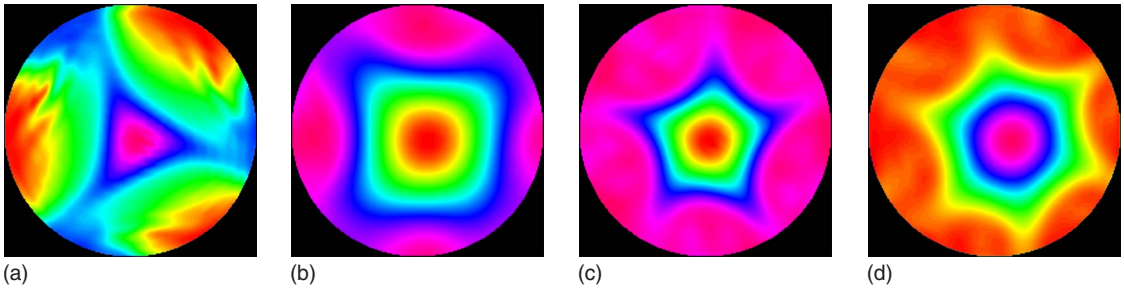

FIG. 3. (Color online) Examples of mode locking of strange eigenmodes to Arnol'd tongues at $\mathrm{Pe}=10^3$ for (a) $\Theta=\frac{2\pi}{3}$, (b) $\Theta=\frac{2\pi}{4}$, (c) $\Theta=\frac{2\pi}{5}$, and (d) $\Theta=\frac{2\pi}{6}$.

spectra. This spectrum evolves via Eq. (2) as

$$\frac{1}{2}\frac{d\alpha_n^2}{dt}=\sum_m \hat{H}_{m,n}\alpha_m\alpha_n-\frac{\mu_n^2}{\mathrm{Pe}}\alpha_n^2, \tag{28}$$

where the advection operator $\hat{H}_{m,n}$ for chaotic flows acts to transfer energy from low to high wave numbers, whereas diffusion acts to remove energy across the spectrum at a rate which scales with the square of the wave number. Although higher wavenumber modes can be populated by $\hat{H}_{n,m}$ without limit (i.e., creation of striations through stretching and folding), these eventually cannot be sustained due to excessive diffusion, as is reflected in a healing of two striations. As eigenmodes driven by a temporally periodic velocity field must be either periodic subharmonic or quasiperiodic; such eigenmodes must *persist* and so the transfer of scalar energy by these mechanisms must balance over a flow period, and so if diffusion is strong, few striations in chaotic flows can persist.

Hence at low Pe, chaotic flows which would otherwise generate high wavenumber eigenmodes can result in lower wavenumber distributions than regular flows at the same Pe. This is reflected in Figs 5 and 6, which respectively show the energy spectra for chaotic and regular RPM stirring protocols at various $\mathrm{Pe}=10^3$ and $\mathrm{Pe}=10^4$. The chaotic spectrum changes markedly due to the fact that the highly striated structure is not sustainable at low Pe, whereas the corresponding spectra for a regular flow shows little change with Pe. For the RPM flow, the mode-locked Hamiltonian for low τ and small, odd j generates rotationally symmetric eigenmodes (Fig. 3) with robust features (with respect to diffusion) which persist at low Pe, and so such regular stirring protocols are globally optimal at such Pe. In general chaotic flows only deliver significantly accelerated scalar dispersion in the so-called advection-dominated regime [6] ($\mathrm{Pe}\gtrsim 10^3$), where higher wave numbers can be maintained, and conversely may be suboptimal with respect to regular flows for $\mathrm{Pe}\lesssim 10^3$.

For all Pe, the distribution of q exhibits horizontal "striping" in the region above $\tau\sim 2$, which become increasingly refined with Pe as per Fig. 2. The distribution of q at $\mathrm{Pe}=10^4$ shown in Fig. 7(a) (with τ now scaled linearly) closely matches the so-called "stability map" [Fig. 7(b)] for the RPM flow [8]. The black regions of the stability map correspond to parameter values which give rise to stable period-1 fixed points in the domain $\mathcal{D}$ for the kinematic problem Eq. (1). These period-1 points occur at the origin at $\tau=2n/3$ for integer values of n, where they are always elliptic and so are associated with nonmixing island structures. With increasing τ, the points can undergo a series of period-doubling bifurcations as the stable islands break down to space-filling chaos before leaving the domain $\mathcal{D}$. The horizontal bands in Fig. 7(b) arise from stable period-1 points prior to period doubling, whereas the steplike structure on the low-Θ region of Fig. 7(b) corresponds to regions where the elliptic points do not bifurcate at all.

Note that the RPM flow also exhibits a period-halving cascade where chaotic points converge initially to periodicity

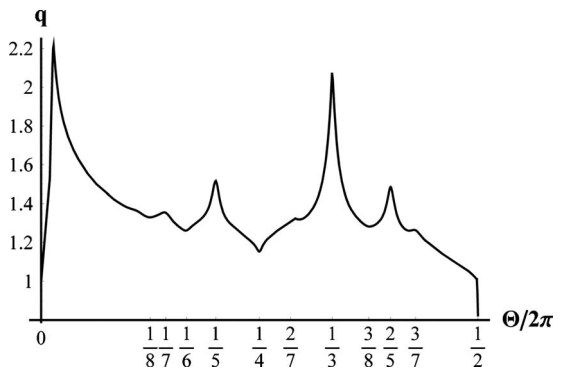

FIG. 4. Influence of mode locking upon transport enhancement q along Θ at low τ (0.01) for $\mathrm{Pe}=10^1$.

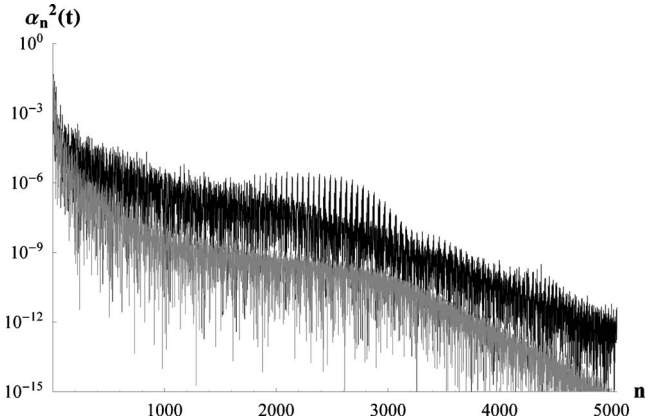

FIG. 5. Strange eigenmode scalar energy spectrum for chaotic mixing protocol at $\mathrm{Pe}=10^4$ (black) and $\mathrm{Pe}=10^3$ (gray).

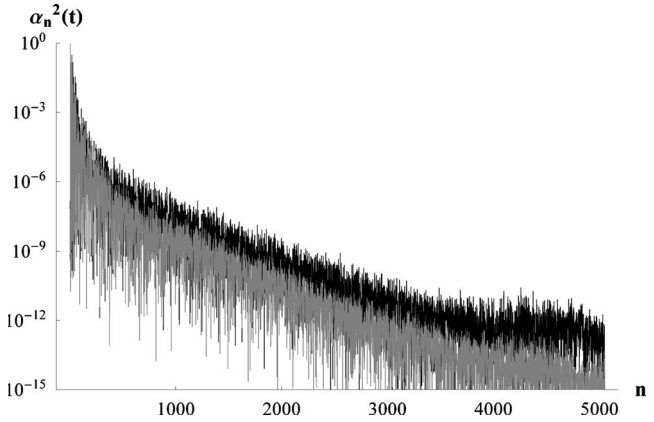

FIG. 6. Strange eigenmode scalar energy spectrum for regular mixing protocol at $\mathrm{Pe}=10^4$ (black) and $\mathrm{Pe}=10^3$ (gray).

and ultimately period halve to a stable elliptic point with increasing τ. These resultant elliptic points give rise to a second stability map, however as the associated island structures are typically very small and close to the boundary $\partial\mathcal{D}$ [8], reverse-cascade elliptic points do not appear to have an effect on the distribution of q over $\mathcal{Q}$.

From Fig. 7, the absence of period-1 points in the kinematic problem (1) corresponds very well with optimal regions of scalar transport at high Pe for the advection diffusion Eq. (2), suggesting elliptic islands do represent

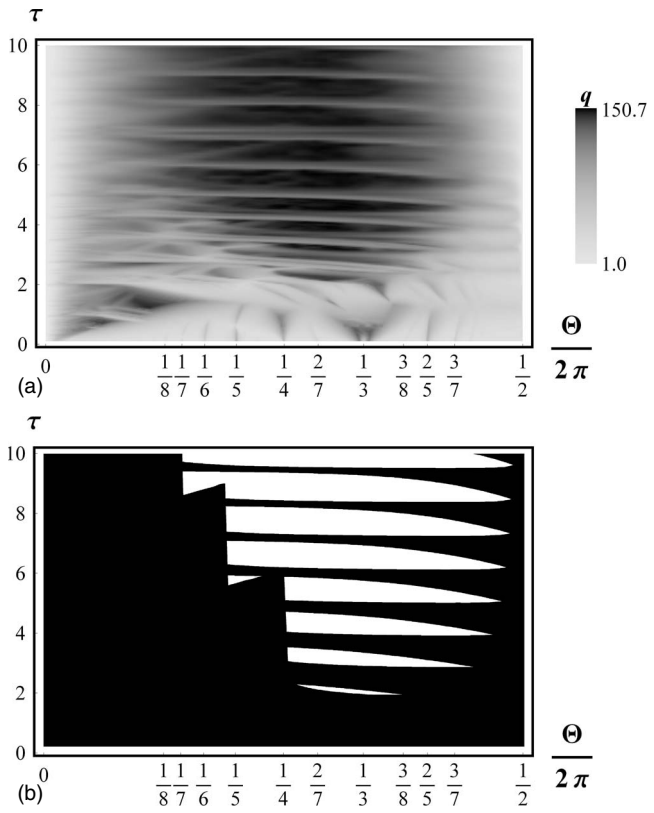

FIG. 7. Correspondence between (a) distribution of dispersion rate q across $\mathcal{Q}$ for $\mathrm{Pe}=10^4$ and (b) instability bands of the RPM flow, where the white regions denote the absence of a period-1 elliptic point for the kinematic problem Eq. (1).

significant barriers to transport in the advection-dominated regime. With decreasing Pe, these bands in q broaden and coalesce, suggesting that resonances due to periodicity of reinjected fluid parcels do persist. At $\mathrm{Pe}=10^4$ the stability bands map directly to the regions of low q, suggesting that further increases in Pe do not refine these structures further, and so these locally optimal regions are parametrically robust with increasing Pe. The distribution of q also corresponds well with the distribution of the Lyapunov exponent over $\mathcal{Q}$ calculated in [8], such that optima are centered about $\tau\sim 2\pi/3$ in the range $\tau=2-5$. At higher values of τ the increased time between reorientation events reduces the amount of folding of striations and so q decays to 1 for large τ.

Figure 8 shows the distribution of $\tau\lambda_0^i$ over $\mathcal{Q}$ for $\mathrm{Pe}=10^1-10^4$, where $\tau\lambda_0^i$ reflects the temporal periodicity of eigenmodes in real space against the RPM offset period τ. Hence for $\tau\lambda_0^i=0$, the eigenmodes are purely real, whereas for $\tau\lambda_0^i\neq 0$ they form complex conjugate pairs (Fig. 9) which are subharmonic for $\lambda_0^i\tau/\pi$ rational or quasiperiodic for $\lambda_0^i\tau/\pi$ irrational. For finite-precision calculations it is impossible to gauge whether $\lambda_0^i\tau/\pi$ is truly irrational, however from Fig. 8 distinct regions of either constant $\tau\lambda_0^i$ or smoothly varying $\tau\lambda_0^i$ are apparent, and so it is argued that the smoothly varying regions contain irrational values of $\tau\lambda_0^i/\pi$ and so correspond to quasiperiodic eigenmodes. Boundaries between all regions (quasiperiodic, subharmonic, and real) correspond to bifurcations in the dominant eigenmode across parameter space $\mathcal{Q}$. As regions of $\tau\lambda_0^i=0$ or $\tau\lambda_0^i=\pi$ covers most of the space $\mathcal{Q}$ in Fig. 8, period-doubling bifurcations from purely real eigenmodes to doubly-periodic eigenmodes (and vice versa) is the most common bifurcation.

At low Pe, the eigenmodes are complex in the limit $\tau\to 0$, with $\tau\lambda_0^i\to\Theta$ (Fig. 8). These eigenmodes tend to become real with increasing Pe, with odd values of j for rational $\Theta/2\pi=k/j$ tending to be real and even j tending complex, as is most clearly evident in Fig. 8(b), where all values of j correspond to mode-locked tongues which exhibit rotationally symmetric eigenmodes (Fig. 3).

Common to all local maxima in q in Fig. 2 is a corresponding bifurcation as reflected in a change in region in Fig. 8. This is especially clear at low Pe where the distributions in $\mathcal{Q}$ are more regular, however the behavior appears to be common across all Pe. For example, the global optimum in $\mathcal{Q}$ for $\mathrm{Pe}=10^4$ occurs at a bifurcation from real to doubly-periodic eigenmodes, the real and imaginary ones of which are shown in Fig. 9. As such, tracking of subharmonic bifurcations may present opportunities to develop new optimization methods which do not require the full resolution of $\mathcal{Q}$, but rather utilize parameter space marching routes which adhere to this bifurcation boundary. The complicated nature of the distribution of q suggests high-density global resolution of $\mathcal{Q}$ is necessary for robust optimization, and so for more complex flows the possibility of more efficient optimization routines are welcome. The optimal value of q over $\mathcal{Q}$ for $\mathrm{Pe}=10^4$ is 150.7, illustrating that simple reorientation alone of the base dipole flow can result in scalar dispersion acceleration of more than two orders of magnitude, significantly higher than corresponding value (11.6) at the same Pe for

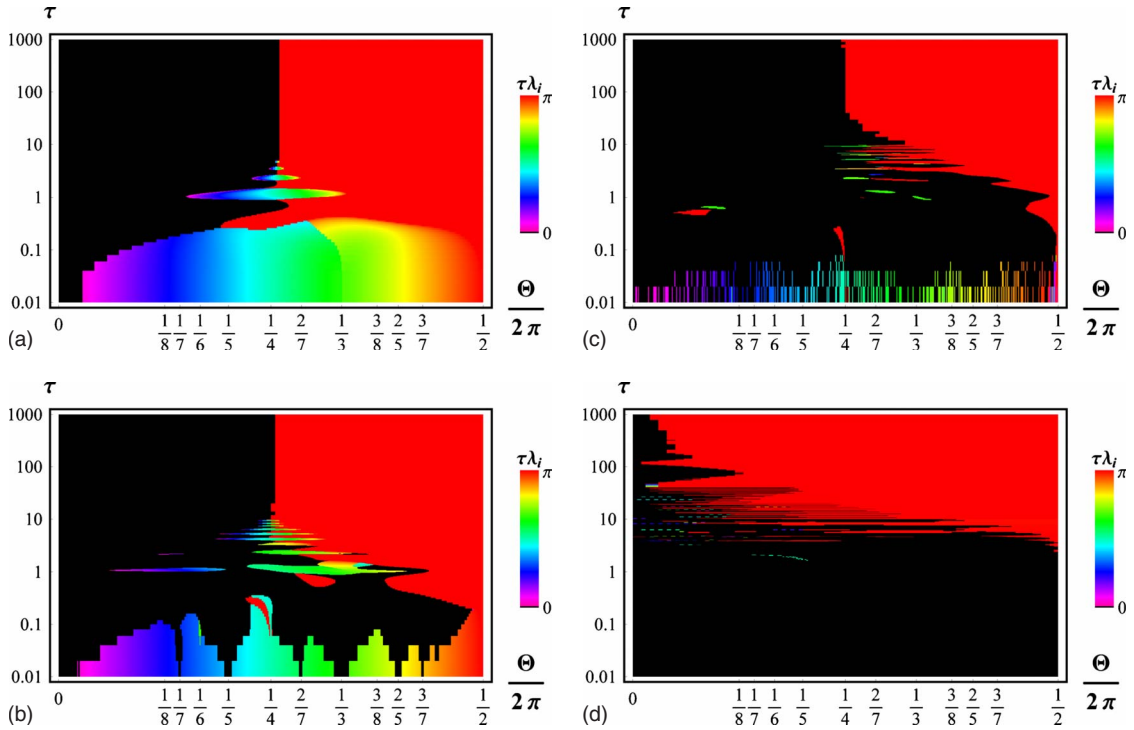

FIG. 8. (Color online) Distribution of the complex eigenmode wavelength $\tau\lambda_i$ over flow parameter space $\mathcal{Q}$ for (a) $\mathrm{Pe}=10^1$, (b) $\mathrm{Pe}=10^2$, (c) $\mathrm{Pe}=10^3$, and (d) $\mathrm{Pe}=10^4$.

other robustly optimized chaotic Stokes flows [24]. These results suggest that significant enhancement of scalar dispersion is possible for potential flows, and presently there exist no known barriers to application of scalar enhancement to potential flows in general. To our knowledge, there are no known studies of Lagrangian chaos or scalar dispersion enhancement thereof in three-dimensional (3D) potential flows, however the extension to three spatial dimensions does not introduce any barriers to the attainment of Lagrangian chaos. The irrotational nature of potential flows in 3D persists, and so unsteady flow is necessary to create heteroclinic or homoclinic connections, unlike 3D steady flows such as the *ABC* flow [25] which are steady and chaotic.

B. Implications for porous media

While applications of potential flow exist in microfluidic mixing and transport [14], another significant field of application is that of scalar transport enhancement in porous media, an area which to date has received little attention in chaotic advection. The connection between porous media flow and potential flow occurs via the Darcy equation at the *macroscale*, and so the results herein apply to porous media systems at such length scales. The scope of this study corresponds to ideal porous media in 2D with homogeneous porosity and permeability distributions, with hydrodynamic dispersion modeled as Brownian diffusion. Clearly more appropriate models are required for porous media applications, however Lagrangian chaos is expected to arise in 3D and/or heterogeneous porous media as the mechanisms to create heteroclinic or homoclinic connections persist.

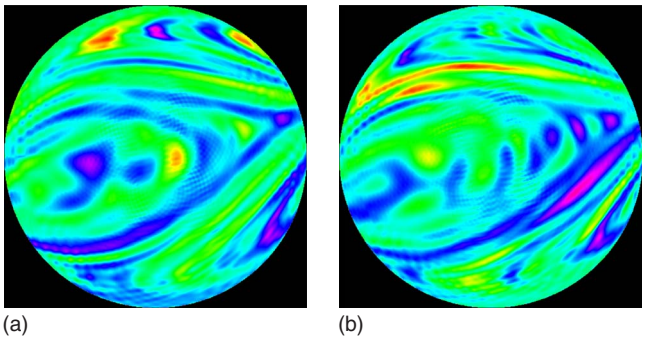

FIG. 9. (Color online) (a) Real and (b) imaginary optimal strange eigenmodes at bifurcation point for $\mathrm{Pe}=10^4$.

Heterogeneous porous media introduces distributions in both porosity and permeability, both of which have significant impacts upon the transport dynamics in porous media. The volume fraction distribution ϵ in heterogenous media renders the macroscopically averaged velocity field $\mathbf{v}$ no longer divergence free, destroying the Hamiltonian and hence conservative nature of the dynamical system (1). As ϵ is steady and satisfies the transport equation $D\epsilon/Dt=0$, the volume averaged velocity $\acute{\mathbf{v}}\equiv\epsilon\mathbf{v}$ is divergence free, and so the system is Hamiltonian with respect to this velocity field. Likewise the ADE for the scalar ϕ is now conservative with respect to $\epsilon\phi$

$$\epsilon\frac{\partial\phi}{\partial t}+\acute{\mathbf{v}}\cdot\nabla\phi=\frac{1}{\mathrm{Pe}}\nabla\cdot(\epsilon\nabla\phi), \tag{29}$$

and so the Lagrangian topology of such flows is dictated by the Hamiltonian structure of $\acute{\mathbf{v}}$ and so accelerated scalar dispersion as quantified by Eq. (29) is expected to persist, in a manner similar to that explored by Speetjens [26].

Heterogeneous permeability generates rotation in Darcy flows as the vorticity $\boldsymbol{\omega}=\boldsymbol{\nabla}k\times\boldsymbol{\nabla}p$ (where p is the flow potential and k the permeability field) is now nonzero. However, Sposito [27] shows that steady 3D heterogeneous flows still have zero helicity (defined as the integral of $\mathbf{v}\cdot(\boldsymbol{\nabla}\times\mathbf{v})$ over the flow domain), and so such porous media flows still cannot exhibit chaotic dynamics [28]. Again, the introduction of transient flow is necessary to generate Lagrangian chaos in 3D and/or heterogeneous porous media. Note that these results apply at the macroscale; steady porous media flows are Stokesian (and possibly have nonzero helicity) at the microscale (where the full tortuosity of the pore structure is resolved), and so give rise to Lagrangian chaos which manifests as hydrodynamic dispersion at the macroscale [29].

Macroscopic modeling of hydrodynamic dispersion is a field of ongoing research, with common models involving longitudinal and transverse (with respect to the velocity direction) diffusion terms which scale with velocity. Such coupling of hydrodynamic dispersion with velocity is fundamentally different to the Brownian diffusion represented as a Laplacian operator in Eq. (2), and the nature of scalar dispersion due to Lagrangian chaos is expected to be qualitatively different. Although extension to three spatial dimensions, hetereogeneous porosity and permeability and non-Brownian diffusion are expected to alter the nature of both Lagrangian chaos and scalar dispersion in porous media, the gross mechanics of dispersion in potential flows is anticipated to persist, as the fundamental mechanism of the creation of transverse heteroclinic or homoclinic connections can still be created by the necessary condition of the transient crossing of streamlines. Certainly quantitative differences in scalar dispersion are expected, however the significant acceleration for 2D potential flows at high Pe generates confidence in the ability to achieve significant results in other systems.

V. CONCLUSIONS

The aim of this work is to determine the potential for Lagrangian chaos to accelerate scalar dispersion in potential flows and identify governing mechanisms. To do so we resolve the dominant strange eigenmode φ_0 and associated decay rate λ_0 of the advection-diffusion operator for a model potential flow (the RPM flow) over the flow control parameter space $\mathcal{Q}$ for various Peclét numbers over $\mathrm{Pe}=10^1-10^4$. The decay rate λ_0 quantifies the asymptotic rate of scalar dispersion, and is shown to exhibit rich behavior over $\mathcal{Q}$, with mode-locking, period-doubling transitions to chaos and fractally distributed maxima observed. The underlying Lagrangian topology [8] of the mixing template plays a major role in the programming of the eigenmodes, which manifest from the interplay between the advection (stretching and folding) and diffusion (healing) operators. Indeed, at large Pe, the distribution of λ_0 over $\mathcal{Q}$ reflects both the symmetry conditions which constrain the Lagragian topology of the RPM flow, and the "instability bands" [8] which denote the absence of stable (elliptic) period-1 points for the kinematic problem is also evident. The global optimum at $\mathrm{Pe}=10^4$ sits on such a band, and this property is anticipated to persist at higher Pe.

The global (with respect to $\mathcal{Q}$) optimum transitions from regions of fully regular (integrable) Lagrangian topologies to chaotic regions around $\mathrm{Pe}\sim 10^3$, suggesting that chaotic advection is only beneficial in the advection-dominated regime [6]. Such behavior is explained by the fact that the short length scale (striated) scalar distributions programmed by chaotic advection cannot be sustained at moderate Pe, however the more regular structures (such as the rotationally symmetric eigenmodes on mode-locked tongues) programmed by nonmixing flows can be sustained in this range and so exhibit faster scalar dispersion. It is believed that such features are generic to scalar dispersion in flows which exhibit Lagrangian chaos, and it is hypothesized that chaotic dynamics are always optimal at large ($\gtrsim 10^4$) values of Pe. The results herein suggest significant enhancements for the model RPM flow, where a 150-fold acceleration is observed at $\mathrm{Pe}=10^4$, with the optimized acceleration scaling as $\sqrt{\mathrm{Pe}}$. Similar enhancements extend to unsteady 2D potential flows in general, so long as scope exists for flow parameters to achieve global Lagrangian chaos. These results indicate Lagrangian chaos to be a viable methodology to achieve process enhancement in such flows.

The similarities between potential and Darcy flows motivate us to consider application of scalar dispersion acceleration via Lagrangian chaos in porous media. Such applications introduce considerations including heterogeneous permeability and porosity and non-Brownian hydrodynamic dispersion. As the fundamental ingredients of Lagrangian chaos persist for such systems given the transient crossing of streamlines, significant acceleration of scalar dispersion is also expected to be possible. Clearly a significant body of work is required to quantify and understand accelerated scalar dispersion in heterogeneous systems, however this represents an important group of studies which shall help bridge the gap between theoretical studies of potential flows and application to a wide range of subsurface industries, including geothermal energy, *in situ* mining, groundwater remediation, and shale oil recovery.

Clearly for more complex flow scenarios such those found in natural geophysical systems, a detailed resolution of $\mathcal{Q}$ may not be feasible, however the overarching linearity of Darcy flows still facilitates exploitation of the underlying symmetries which deliver the efficiencies of the composite spectral method [15]. Observations that local optima in $\mathcal{Q}$ lie along bifurcation boundaries between regular and subharmonic or quasiperiodic eigenmodes points to novel methods to optimize the stirring protocol which does not require detailed global resolution of $\mathcal{Q}$. Such behavior is also observed in Stokes flows [7], and so point to novel optimization methods for such systems in general.

The admission of Lagrangian chaos in porous media also opens lines of research into unlocking complex geophysical phenomena such as ore body formation and mineral deposition. It is likely that in certain geophysical scenarios chaotic advection has an important role to play in the transport and dispersion of chemical and mineral species, and it is postulated that resonance effects may be responsible for the creation of large local depositions and the highly nonuniform distribution of ore throughout the rock matrix. A more thorough understanding of the nature and mechanisms of La-

grangian chaos in heterogeneous media is required to answer such questions, however the persistence of naturally occurring periodic forcings over geological time scales suggests some likelihood of the presence of chaotic dynamics. Resolution of scalar transport dynamics over the parameter space $\mathcal{Q}$ may prove useful for the forward problem of optimization of a geoengineering application, and also may provide a means of tackling the inverse problem of determining what potential subsurface processes have led to observed mineral distributions.

[1] H. Aref, J. Fluid Mech. **143**, 1 (1984).
[2] J. M. Ottino, *The Kinematics of Mixing: Stretching, Chaos and Transport* (Cambridge University Press, Cambridge, 1989).
[3] X. Z. Tang and A. H. Boozer, Phys. Fluids **11**, 1418 (1999).
[4] V. Ganesan, M. D. Bryden, and H. Brenner, Phys. Fluids **9**, 1296 (1997).
[5] V. Toussaint, P. Carrière, J. Scott, and J.-N. Gence, Phys. Fluids **12**, 2834 (2000).
[6] A. Adrover, S. Cerbelli, and M. Giona, Comput. Chem. Eng. **26**, 125 (2002).
[7] D. Lester, M. Rudman, and G. Metcalfe, Int. J. Heat Mass Transfer **52**, 655 (2009).
[8] D. R. Lester, G. Metcalfe, M. G. Trefry, A. Ord, B. Hobbs, and M. Rudman, Phys. Rev. E **80**, 036208 (2009).
[9] S. W. Jones and H. Aref, Phys. Fluids **31**, 469 (1988).
[10] G. Metcalfe, D. R. Lester, A. Ord, P. Kulkarni, M. Rudman, M. Trefry, B. Hobbs, K. Regenaur-Lieb, and J. Morris, Philos. Trans. R. Soc. London, Ser. A (in press).
[11] G. Metcalfe, D. Lester, A. Ord, P. Kulkarni, M. Trefry, B. E. Hobbs, K. Regenaur-Lieb, and J. Morris Philos. Trans. R. Soc. London, Ser. A **368**, 217 (2010).
[12] P. Zhang, S. L. Devries, A. D. Dathe, and A. C. Bagtzoglou, Environ. Sci. Technol. **43**, 6283 (2009).
[13] S. M. Cox, P. G. Drazin, S. C. Ryrie, and K. Slater, J. Fluid Mech. **214**, 517 (1990).
[14] M. Stremler and B. Cola, Phys. Fluids **18**, 011701 (2006).
[15] D. Lester, M. Rudman, G. Metcalfe, and H. Blackburn, J. Comput. Phys. **227**, 3032 (2008).
[16] D. Rothstein, E. Henry, and J. P. Gollub, Nature (London) **401**, 770 (1999).
[17] W. Liu and G. Haller, Physica D **188**, 1 (2004).
[18] R. T. Pierrehumbert, Chaos, Solitons Fractals **4**, 1091 (1994).
[19] P. J. Schmid, Annu. Rev. Fluid Mech. **39**, 129 (2007).
[20] D. Levin, J. Comput. Appl. Math. **67**, 95 (1996).
[21] W.-X. Zhong, J. Comput. Appl. Math. **163**, 59 (2004).
[22] G. Metcalfe, *Complex Physical, Biophysical, and Econophysical Systems*, Lecture Notes in Complex Systems Vol. 9 (World Scientific, New York, 2010), p. 187.
[23] J. A. Glazier and A. Libchaber, IEEE Trans. Circuits Syst. **35**, 790 (1988).
[24] D. R. Lester, G. Metcalfe, and M. Rudman, 13th International Heat Transfer Conference, Sydney, Australia, 2006 (unpublished).
[25] D.-B. Huang, X.-H. Zhao, and H.-H. Dai, Phys. Lett. A **237**, 136 (1998).
[26] M. F. M. Speetjens, Phys. Rev. E **77**, 026309 (2008).
[27] G. Sposito, Water Resour. Res. **30**, 2395 (1994).
[28] D. D. Holm and Y. Kimura, Phys. Fluids A **3**, 1033 (1991).
[29] J. M. Ottino, Annu. Rev. Fluid Mech. **22**, 207 (1990).